ISSN1027-5495. Functional Materials, 31, No.4 (2024), p. 574-586
doi:http://dx.doi.org/10.15407/fm31.04.574

Optimization of CZT crystal growth by THM method

S. Galkin, O. Kolesnikov, I. Rybalka, O. Lalayants

Institute for Scintillation Materials of the National Academy of Sciences of Ukraine

Received September 1, 2024

This work develops a numerical model for analyzing the growth conditions of $Cd_{0.9}Zn_{0.1}Te$ crystals by the traveling heater method (THM) in a multi-zone electrodynamics gradient (EDG) furnace. The main focus is on determining the temperature profile and the thickness of the Te-rich solution to improve the structural homogeneity of the crystals and minimize defects. The work also proposes a dimensionless criterion based on the ratio of the thermal Rayleigh number (Ra_T) to the concentration Rayleigh number (Ra_C), which allows for evaluating the growth conditions. The calculations performed make it possible to determine the main technological parameters that ensure a nearly flat crystallization interface. The adequacy of the calculated thermal conditions was confirmed experimentally. The obtained samples showed characteristics suitable for manufacturing spectroscopic grade detectors.

Keywords: CZT, THM method, numerical model, growing conditions.

Оптимізація процесу вирощування кристалів CZT методом THM. *С. Галкін, О. Колесніков, І. Рибалка, О. Лалаянц*

У цій роботі розроблено чисельну модель для аналізу умов вирощування кристалів $Cd_{0.9}Zn_{0.1}Te$ методом рухомого нагрівача у багатозонній електродинамічній градієнтній печі. Основна увага приділена визначенню температурного профілю і товщини розчину, збагаченого телуром, для покращення структурної однорідності кристалів і мінімізації дефектів. В роботі також запропоновано безрозмірний критерій, заснований на відношенні теплового числа Релея (Ra_T) до концентраційного числа Релея (Ra_C), який дозволяє оцінити умови росту. Проведені розрахунки дозволяють визначити основні технологічні параметри, які забезпечують практично плоску поверхню кристалізації. Достовірність розрахованих теплових режимів підтверджено експериментально. Отримані зразки показали характеристики, придатні для виготовлення детекторів спектроскопічного класу.

1. Introduction

Semiconductor materials based on CdTe, as well as CdTe-ZnTe solid solutions, are widely used in various fields of radiation instrumentation. This is due to their advantages over traditional scintillation materials, such as a high atomic number ($Z_{eff} = 50$) [1, 2], excellent energy resolution [3, 4], and a wide bandgap (compared to high-purity germanium) of about 1.44–1.57 eV [2], allowing for the fabrication of highly efficient detectors that operate without cryogenic cooling [5]. Due to these properties, CdTe-based detectors are widely used in spectrometry [6], astrophysics [2, 5], nuclear safety systems [7], medical imaging devices [2, 8], environmental radiation monitoring [9], etc. One of the most in-demand materials is $Cd_{0.9}Zn_{0.1}Te$ (CZT).

Nowadays, CdTe-based crystals are grown by the Bridgman method under high pressure inert gas (HPB) [10 - 12] or by the Traveling Heater Method (THM) [13 - 15]. The Bridgman method belongs to the class of melting methods. Growth occurs at temperatures above the melting point of the material (around 1300K).

The typical growth rate is about 1 mm/hr. Since the melt thermally dissociates with preferential carryover of cadmium, special precautions are required to reduce the dissociation effect. In practice, a high pressure of inert gas (0.5-1 GPa) in the atmosphere of the growth furnace [12], or an overpressure of Cd vapor above the melt in the growth furnace are usually used.

The THM method belongs to the class of solution-melt methods. The starting material is dissolved in a layer of molten Te in the central part of the growth ampoule. Crystallization of the ingot occurs from a solution of CdTe in Te. The growth takes place at temperatures that are much lower than the melting temperature of the material (typically 1000-1200K) [13, 14].

The THM method is characterized by relatively low crystal growth temperatures and a low degree of supersaturation at the crystallization interface. Contamination of the melt by products of interaction with the crucible material is also reduced [2]. The stoichiometry of the crystal is less disturbed. At the same time, the THM method has several disadvantages, namely: the optimal growth rate in THM (about 0.1 mm/hr) is significantly lower than in the HPB method; tellurium inclusions are observed in the grown crystals; typical are instabilities of the phase boundary due to the instability of crystallization conditions and the uneven nature of tellurium melt mixing at various stages of growth [3, 16]. To overcome the above disadvantages it is necessary to optimize and carefully control many technological parameters: the temperature distribution profile in the furnace, the thickness of the molten tellurium layer, take into account the thermophysical properties of the crystal crucible and the melt materials, ampoule rotation [13 - 15, 17, 18], etc. For the above mentioned methods of growing CdTe crystals, common problems are inclusions of the Te phase, the presence of a network of subgrain boundaries and non-uniform chemical composition of the grown ingot [10 - 15].

Achieving and maintaining a specific shape of the phase boundary is one of the main criteria determining the acceptability of growth conditions. The best results were obtained with a flat or slightly convex crystallization interface. A concave crystallization front shape is often a cause of parasitic crystallization near the crucible wall and the formation of grains. One of the key parameters affecting the structural homogeneity of the ingots is the thickness of the Te-rich solution zone [18].

Earlier, the need for optimizing the axial temperature gradient in the Te-rich solution zone to reduce the influence of turbulent convection was noted. It was found that a temperature gradient greater than 20 K/cm increases the likelihood of turbulent convection in the melt, which negatively affects the structural quality of the grown ingots [19].

In recent decades, a considerable number of studies have been published on the numerical modeling of the CdTe-based crystal growth process using the traveling heater method (THM). The works [19-24] present the results of modeling heat and mass transfer processes during crystal growth by THM. However, the design of the thermal unit and the type of growth setup are not disclosed, and the temperature distribution on the ampoule wall is specified directly as a boundary condition. In [4, 25, 26], setups with three heating zones are considered, in which a separate heater creates the required temperature distribution in the Te-rich solution zone. In this case, the characteristics of the thermal field and growth conditions are determined by the design of the heater.

More modern furnaces are electrodynamics gradient (EDG H_2O) furnaces. Structurally, this is a multi-zone furnace containing several dozen independent heaters. The creation of a specified thermal distribution and its movement relative to the growth ampoule is achieved through coordinated changes in the temperatures of all the heaters, eliminating the need for mechanical movement of the ampoule. This is one of the main advantages of EDG furnaces. There are known studies on the numerical modeling of CdTe-based crystal growth in EDG furnaces. However, most of them refer to the Bridgman melting method [27 - 30], high-pressure gradient freezing [31], and the vertical gradient freezing [32]. At the same time, very few studies are known that are dedicated to modeling global heat transfer in EDG furnaces using the THM method. The work [33] is devoted to studying the influence of crucible temperature and crucible rotation on the shape of the crystallization interface for A_3B_6 compounds.

A specific limitation of EDG furnaces is their inability to create a sufficiently high and controllable temperature gradient in a narrow region. This is due, in particular, to several factors. It is impractical to reduce the width of an individual heater and increase the total number of heaters in the growth furnace beyond

reasonable limits. Radiation heat transfer and convective flows in the air gap between heaters and the ampoule contribute to the broadening of the temperature peak. This effect becomes especially noticeable when the difference between the diameters of the furnace and the ampoule increases. This makes it difficult to create a narrow temperature peak with a high gradient required in the Te-rich solution zone.

From a practical point of view, the task of optimizing thermal growth conditions comes down to determining the required thickness of the Te-enriched solution layer and creating an appropriate temperature distribution across the heaters of the multi-zone furnace, given the specified ampoule diameter and furnace design. Experimental determination of these parameters is a complex and time-consuming process, so numerical modeling of global heat exchange processes is a valid approach. The global model should take into account both heat and mass transfer processes at the crystallization interface, as well as radiation and convective heat transfer between the furnace and the ampoule.

Thus, despite the widespread use of the THM method for crystal growth and numerous studies on heat transfer processes, the growth of $Cd_{0.9}Zn_{0.1}Te$ single crystals in multi-zone EDG furnaces using the THM method remains insufficiently covered in the literature.

The aim of this work is to develop and implement a numerical model for optimizing the growth conditions of $Cd_{0.9}Zn_{0.1}Te$ single crystals by the traveling heater method (THM) in a multi-zone EDG furnace. The main focus is on selecting the temperature profile and the thickness of the Te-rich solution layer to improve the structural homogeneity of the crystals and minimize defects. The primary criterion was to achieve a nearly flat crystallization interface. The calculated thermal conditions were verified by experimental studies.

2. Experimental procedure

2.1. Materials and methods

$Cd_{0.9}Zn_{0.1}Te$ ingots with a diameter of 40 mm were grown in quartz ampoules in a multi-zone EDG furnace using the THM method. The geometry of the growth setup is schematically shown in Fig. 1. The model includes both solid and fluid blocks. The solid blocks consist of heaters, thermal insulation, ampoule, crystal (CZT_{CR}), and starting material (CZT_{SM}).

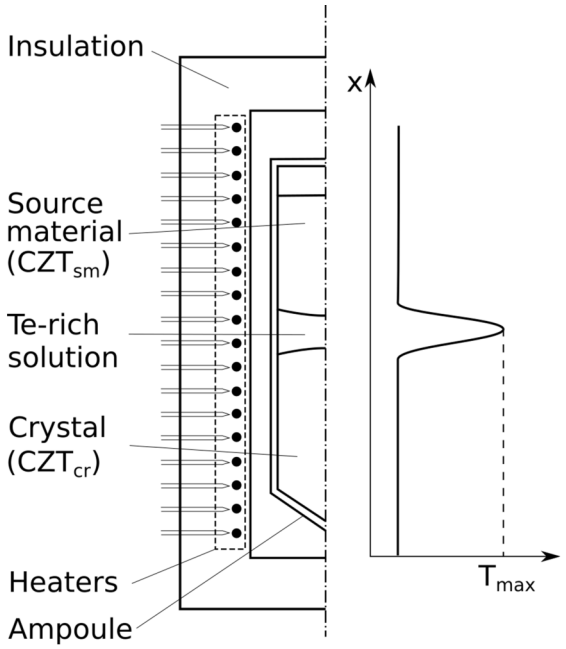

Fig. 1. Schematic diagram of the furnace and temperature distribution in the THM method.

In the experiments on growing $Cd_{0.9}Zn_{0.1}Te$ ingots, the starting elements Cd, Zn and Te with a purity of 6N were used as raw materials. The ingots were cut using a diamond wire saw. The surfaces of the plates and detector faces were polished according to the method described in [34].

X-ray phase analysis of powders was carried out using a SmartLab SE X-ray diffractometer from Rigaku. The diffraction patterns were obtained using Cu-$K\alpha$ radiation at U = 40 kV, I = 50 mA. Data analysis was performed using the Rietveld method.

Structural defects in the crystals were studied using a high-sensitivity Shimadzu AIM-9000 microscope (signal-to-noise ratio 30,000:1) in the optical and infrared spectral ranges. To reveal microstructural defects in the studied crystals, the method of chemical selective etching was applied. The following compositions and etching modes were used [35]: for chemical polishing – 10 ml of concentrated HNO_3, 25 ml of H_2O, 4 g of $K_2Cr_2O_7$, temperature 308 K, time 30 s; for dislocation etching – 10 ml of polishing solution, 2 ml of concentrated HNO_3, 15 mg of $AgNO_3$, temperature 333 K, time 60 s.

2.2. Model

Governing equations

The governing equations are as follows:

$$\rho A_p \left[\frac{\partial T}{\partial t} + (\bar{u} \cdot \nabla) T \right] = k \nabla^2 T \ , \qquad (1)$$

$$\frac{\partial \rho \bar{u}}{\partial t} + (\bar{u} \cdot \nabla)\rho \bar{u} = -\nabla \bar{p} + \nabla \cdot \tau + \\ + \rho g\left[1 - \beta_T (T - T_0) + \beta_C (C - C_0)\right], \quad (2)$$

$$\frac{\partial \rho}{\partial t} + \nabla \cdot (\rho \bar{u}) = 0 , \quad (3)$$

$$\tau_{ij} = \mu_{eff}\left(\nabla \bar{u} + \nabla \bar{u}^T\right) - \frac{2}{3}\mu_{eff}\delta_{ij}\nabla \cdot \bar{u} , \quad (4)$$

$$\mu_{eff} = \mu + \mu_t , \quad (5)$$

$$\mu_t = A\frac{K^2}{E} , \quad (6)$$

$$\rho = \frac{p_0 M}{RT} , \quad (7)$$

where: ρ is the density; c_p is the heat capacity; t is the time; k is the thermal conductivity; T is the temperature; T_0 is the reference temperature; C_0 is the reference concentration; β_T is the volumetric thermal expansion coefficient; β_S is the solutal volume expansion coefficient; $\bar{u}$ is the filtered instantaneous velocity field; $\bar{p}$ is the filtered instantaneous pressure field; p_0 is the reference pressure; $\boldsymbol{g}$ is the gravitational vector; μ_{eff} is the effective dynamic viscosity; μ is the dynamic viscosity; μ_t is the turbulent viscosity; A is the closure constant; K is the turbulent kinetic energy; E is the turbulent kinetic energy dissipation rate; τ is the stress tensor; δ_{ij} is the Kronecker delta; M is the molecular weight of the air species; R is the gas constant.

The energy conservation equation (1) is formulated for all blocks of the computational domain. Equations (2)–(6) were applied to both the incompressible molten Te and the air gap region between the ampoule and the furnace walls. The Boussinesq approximation was used. Air was treated as an ideal gas; its density was determined by equation (7).

The liquid and gas flows were considered unsteady and turbulent. A Large Eddy Simulation (LES) model [36] was applied, which assumes spatial filtering of velocity and pressure fields in equations (2) and (3). The filter size is equal to the grid size (implicit LES). Eddies larger than the filter size are computed directly, while smaller eddies are modeled using a subgrid-scale model based on turbulent viscosity, as described by equations (4)–(6) [37]. A one-equation model was used to represent turbulent viscosity.

Radiation heat transfer calculations were performed in the cavity between the inner surfaces of the furnace and the ampoule using the finite volume Discrete Ordinates Method (fvDOM) [38] for a diathermic medium [39].

$$\hat{s} \cdot \nabla I(r, \hat{s}) = \varepsilon(I_b - I), \quad (8)$$

$$q_r = \sum_{i=1}^{n} w_i I_i(r)\hat{s}_i , \quad (9)$$

where: ε is the emissivity; $\boldsymbol{s}$ is the ray direction unit vector; $\boldsymbol{r}$ is the position vector; $\boldsymbol{I}$ is the magnitude of radiation in a specified direction; I_b is the blackbody intensity of radiation; w_i is the directional weights fvDOM; $\boldsymbol{q_r}$ is the radiation flux.

The following assumptions were used: the air in the gap between the ampoule and the furnace walls was treated as a transparent, non-scattering medium. The furnace walls and the ampoule were modeled as opaque, gray, diffuse surfaces with an emissivity coefficient of ε = 0.9. For discretization, the polar angle in the range $0 \le \theta \le \pi$ was divided into 15 segments, and the azimuthal angle in the range $0 \le \le 2\pi$ was divided into 30 segments, resulting in a total of 450 discretized solid angles.

Mass transfer is described by the diffusion-convection equation

$$\frac{\partial C}{\partial t} + \nabla \cdot (\bar{u}C) = \nabla \cdot (D_{eff}\nabla C), \quad (10)$$

where $\boldsymbol{u}$ is the tellurium melt velocity field; C is the mass fraction of the dissolved component; D_{eff} is the effective diffusion coefficient.

Initial conditions at $t=0$

$$\begin{cases} T = T_0 \\ C = C_0 \\ u = 0 \end{cases} . \quad (11)$$

Shapes of the Te raw material – melt ($\Gamma_{\text{RM-M}}$) and the Te crystal – melt ($\Gamma_{\text{CR-M}}$) interfaces are assumed to be flat at t=0

$$\Gamma_{RM-M} = Z_{RM} \quad (12)$$

$$\Gamma_{CR-M} = Z_{CR} \quad (13)$$

Boundary at t > 0:

1) Condition at heaters:

$$T = T_i = const , \quad (14)$$

where i = {1, 2, … 30} is the heater number.

This condition corresponds to the operation of the heater temperature regulators in steady-state mode.

2) Condition at the solid-liquid interfaces:

$$n \cdot \left(k_l \nabla T \mid l - k_s \nabla T \mid s\right) = \rho_s \Delta H n \cdot V, \quad (15)$$

where ρ is the density; ΔH is the heat of crystallization; $\boldsymbol{V}$ is the velocity vector of the inter-

Table 1 - Thermophysical properties of materials

Material	Parameter (Symbol)	Units	Value	Ref
CZT solid	Density (ρ)	kg m $^{-3}$	5760	This work
	Thermal conductivity (k)	W/m K	3.1	[41]
	Specific heat (c_p)	J/kg K	160	[42]
	Enthalpy of fusion (ΔH)	J/g	209	[43]
	Lewis number	-	780	[40]
	Prandtl number	-	0.04	[40]
	Solutal diffusion coefficient (D_s)	m^2 c^{-1}	5×10−9	[40]
liquid	Density (ρ)	kg m $^{-3}$	5620	[20]
	Thermal expansion coefficient (β_T)	K^{-1}	0.0005	[44]
	Solutal expansion coefficient (β_C)	mol^{-1}	0.056	[45], [46]
	Thermal conductivity (k)	W/m K	5.7	[20]
	Specific heat (c_p)	J/kg K	372	[20]
	Viscosity of liquid (μ)	Pa s	0.0008992	[20]
Silica ampoule	Density (ρ)	kg m $^{-3}$	2200	[20]
	Thermal conductivity (k)	W/m K	3.1	[20]
	Specific heat (c_p)	J/kg K	770	[20]
Air	Density (ρ)	kg m $^{-3}$	0.2582	[42]
	Thermal expansion coefficient (β_T)	K^{-1}	0.00078	[42]
	Thermal conductivity (k)	W/m K	0.0242	[42]
	Specific heat (c_p)	J/kg K	1212	[42]

facial boundary movement; indices *l, s* denote fluid and solid, respectively.

3) Condition at the boundaries between different blocks within the computational domain is the continuity of temperature and heat flux. For fluid blocks, the no-slip condition is also applied.

$$\begin{cases} T_i = T_j \\ n \cdot (k_i \nabla T \mid i) = n \cdot (k_j \nabla T \mid j). \\ u = 0 \end{cases} \quad (16)$$

4) Condition at the outer surfaces:

$$n \cdot \left(-k \nabla T\right) = \alpha \left(T - T_{amb}\right), \quad (17)$$

where: a is the heat transfer coefficient; T_{amb} is the ambient temperature.

5) Condition at the boundaries of the radiation cavity (the boundaries of the ampoule and the furnace walls):

$$n \cdot \left(k_i \nabla T \mid i\right) = n \cdot \left(k_j \nabla T \mid j\right) + n \cdot q_r. \quad (18)$$

6) The condition for concentration at the boundaries of dissolution (19) and crystallization (20) is based on the assumption of constant concentration in the solid phase (no diffusion). At the dissolution front, the starting material dissolves in the Te-enriched solution, increasing the CZT concentration in the melt, while at the crystallization front, CZT crystallizes from the solution, decreasing the CZT concentration in the melt. Additionally, for simplicity, we assume that CZT does not dissociate in the Te-rich solution [40].

$$-n \cdot D \nabla C \mid l = \rho_s n \cdot V. \quad (19)$$

$$-n \cdot D \nabla C \mid l = -\rho_s n \cdot V. \quad (20)$$

The concentration at the dissolution and crystallization boundaries corresponds to equilibrium

$$C \mid l = C_{eq}. \quad (21)$$

The equilibrium concentration is determined along the liquidus line of the binary phase diagram and is interpolated by a third-degree polynomial:

$$T\left(K\right) = 725.7 + 1630.7814C - \\ -1979.765C^2 + 1004.15C^3, \quad (22)$$

where T and C are the coordinates of the points along the temperature and concentration axes of the liquidus line of the phase diagram [21].

Thermophysical properties of materials are given in Table 1.

Optimization procedures

In this work, two optimization problems need to be solved. The first problem is to find a temperature distribution across the heaters to ensure the desired thermal field inside the

furnace. The second problem is to determine the technological parameters that provide the required shape of the crystallization interface, flow regime, and other conditions.

The procedure for optimizing the temperature distribution inside the furnace

As noted earlier, to implement the THM method in EDG furnaces, it is necessary to determine the temperature distribution across the heaters of the growth furnace in order to achieve the desired temperature distribution over the surface of the ampoule. At the same time, it is important to ensure arbitrary positioning and movement along the furnace axis with minimal deviations. To solve this problem, we create the following model.

Let us define the objective function $F(T_H)$ as the sum of the squared deviations of the temperature values from the required temperatures at each point. The priority of certain points where temperature measurement accuracy is critical will be taken into account by adding penalty coefficients.

$$F(T_H) = \sum_{i=0}^{n} \lambda_i \left(T(x_i) - T_0(x_i) \right)^2 , \quad (23)$$

where T_H is the vector of temperatures set on the heaters; $T(x_i)$ is the calculated temperature at point x_i in the furnace, $T_0(x_i)$ is the target temperature at point x_i in the furnace; λ_i is the penalty coefficients.

To find the optimal parameters of the temperature distribution, we minimize the objective function (20) by the gradient descent method:

$$T_j^{(k+1)} = T_j^{(k)} - \eta \frac{\partial F(T_H)}{\partial T_j} , \quad (24)$$

$$\frac{\partial F(T_H)}{\partial T_j} \approx \frac{F(T_1, T_2, ..., T_j + \Delta T_j, ..., T_{30}) - F(T_1, T_2, ..., T_j, ..., T_{30})}{\Delta T_j} , \quad (25)$$

where $''^{(k)}_j$ is the temperature of the j-th heater at the k-th iteration; η is the gradient descent step; $\frac{\partial F(T_H)}{\partial T_j}$ is the partial derivative of the objective function by the heater temperature T_j; ΔT_j is the temperature increase temperature increase; index j $(j = 1,2,...,30)$ indicates the number of the heater in the furnace.

The gradient descent cycle stops when the convergence condition for all j:

$$\left| T_j^{(k+1)} - T_j^{(k)} \right| < \epsilon , \quad (26)$$

where ϵ is the specified convergence threshold.

The temperature difference limit for the adjacent heaters in the EDG growth furnace is given by the inequality:

$$\left| T_j - T_{j+1} \right| < \delta , \quad (27)$$

where δ is the maximum achievable difference between the temperatures of adjacent furnace heaters, determined experimentally.

Procedure for optimizing process parameters

Considering that: 1) the geometry of the setup and the thermophysical properties of the materials are specified approximately; 2) the goal is to determine several parameter sets close to the optimal ones, which will be verified during the experimental ingot growth; 3) the parameter space considered in this work is quite limited, – optimization by the "brute force" method is preferable to using traditional optimization methods. Another argument in favor of choosing the brute-force method was that the flow regimes and structures of the convective flows were evaluated visually. We considered it impractical to formalize this criterion, which led to the rejection of traditional optimization methods. A series of calculations was performed, in which the temperature distribution profile and the thickness of the Te-enriched solution layer were varied.

Numerical simulation method

An irregular mesh consisting of tetrahedral elements was used for the discretization of the computational domain. The finite volume method (FVM) was applied to solve the equations presented in this work. This is one of the most widely used methods in computational fluid dynamics [47]. The CHTMultiRegion (Conjugate Heat Transfer Multi Region) solver from the OpenFoam package was used [48, 49]. The equations for each variable of the system are solved sequentially. At the fluid-solid interface boundaries, the equations for the fluid are solved first, using the temperature of the solid from the previous iteration as the boundary condition for the temperature. Then the equation for the solid is solved, using the temperature of the fluid from the previous iteration as the boundary condition for the solid. This iterative procedure is performed until convergence is reached [49, 50].

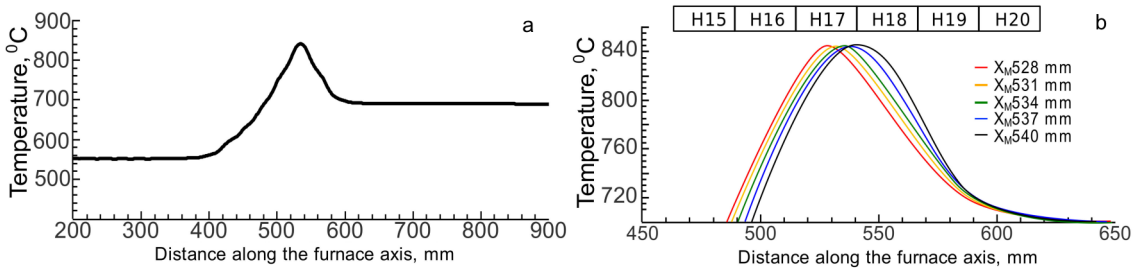

Fig. 2. Temperature distribution along the furnace axis: (a) on the surface of the heating zones (inner wall of the furnace), (b) on the surface of the ampoule during the movement of distribution 2a.

Table 2 - Main characteristics of temperature and flow fields

	Profile 1	Profile 2	Profile 3	Profile 4
Maximum temperature (Tmax), °C	795	807	815	840
Temperature gradient K/cm	5	12,3	21,5	43

Table 3 — Thermal and concentration Rayleigh numbers ratio depending on the thickness of the Te-enriched solution layer and the temperature profile

Te thickness, mm	Profile 1	Profile 2	Profile 3	Profile 4
30	7·10-4	4·10-3	6·10-3	1·10-2
40	9·10-4	8·10-3	1·10-2	3·10-2
50	2·10-3	2·10-2	3·10-2	5·10-2

3. Results and discussion

3.1. Heat distribution in EDG furnaces for the THM method

The following temperature distribution was implemented along the furnace axis (Fig. 2a). In the Te-enriched solution zone, a temperature peak is formed that has an approximately Gaussian shape. After the peak, in the feed material zone, a uniform temperature of 700°C is maintained. Before the peak, a linear temperature gradient is established, providing heat removal from the crystallization interface and creating conditions for ingot annealing. In the lower part of the furnace, a constant temperature of 550°C is maintained.

As already mentioned for EDG furnaces, the movement of the thermal field inside the furnace is created by the redistribution of temperatures between the heaters. Fig. 2b shows the evolution of the shape of the temperature peak on the ampoule wall at five different heater temperature distributions. The maximum temperature of the peak as it moves along the furnace axis remains almost unchanged (changes do not exceed 0.5 °C). The changes in the shape of the peak are more noticeable. When the peak is produced predominantly by one heater (heater H17, position 528 mm in Fig. 2b), it is sharper with a wider base. When the peak is created equally by two heaters (heaters H17 and H18, position 544 mm in Figure 2.b) the peak apex becomes wider and the base narrows. The change in peak width at half maximum is about 10 %.

3.2. Temperature and velocity fields

This section presents the results of numerical calculations performed to determine the influence of the thickness of the tellurium layer and the temperature peak profile on the ratio (Ra_T/Ra_C) of the thermal Rayleigh number (Ra_T) to the concentration Rayleigh number (Ra_C). The primary goal of the calculations was to find a combination of technological parameters that ensures crystal growth conditions close to optimal. Later in this section, a discussion of the influence of this relationship on the flow characteristics in the melt will be presented. We hypothesize that controlling the Ra_T/Ra_C ratio is one of the possible ways to stabilize the crystallization interface, minimize defects, and improve the structural homogeneity of the crystals. As the main process parameters, three thicknesses of the tellurium layer (30, 40, and 50 mm) and four temperature profiles with different amplitudes and gradients were chosen (Table 2). The influence of these parameters on the flow characteristics, and the distribution of thermal and concentration fluxes were analyzed.

Table 3 shows how changes in the thickness of the tellurium layer and the shape of the tem-

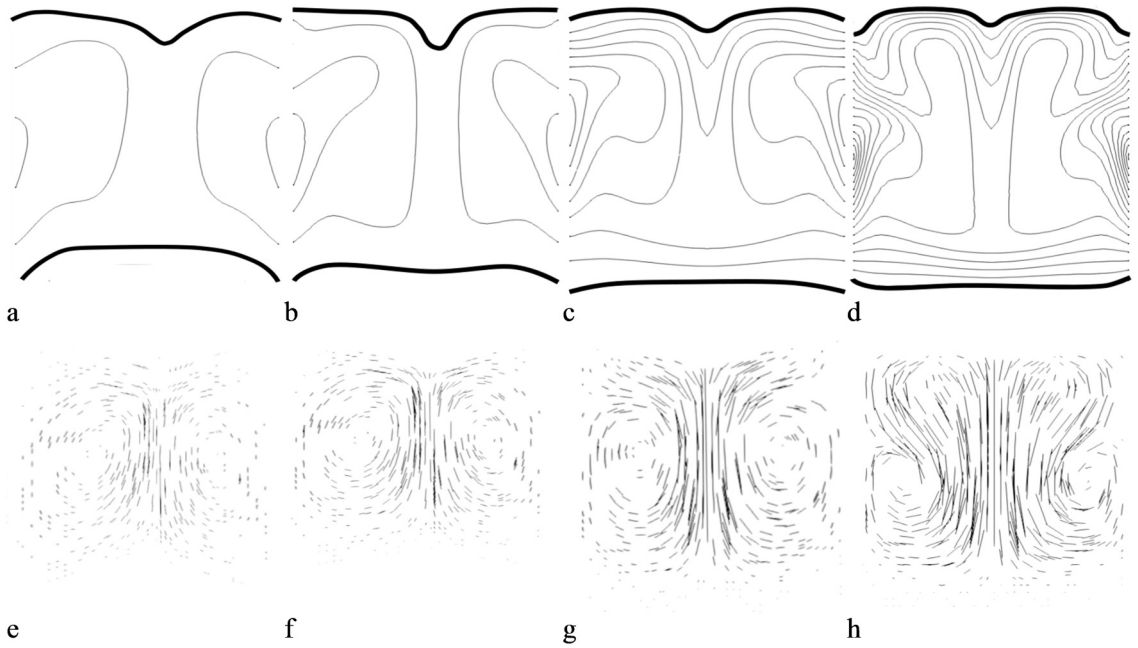

Fig. 3.Temperature distribution and flow structure in the melt with the Te-enriched solution thickness of 40 mm. (a, e-Profile1; b, f-Profile2; c, g-Profile3; d, h-Profile4. The maximum isotherm: a) 793 °C, b) 805 °C, c) 813 °C, d) 838 °C. Step of isotherms 5K).

perature profiles affect the Ra_T/Ra_C ratio. This allows us to separately consider the influence of each parameter on the convection regimes.

Figure 3 shows the flow structure in the Te-enriched solution. The overall flow pattern is determined by buoyancy forces. The upward flow of the solution along the ampoule wall is associated with the higher temperature at the wall. The downward flow is directed along the axis of the ampoule, where the flow velocity is maximal. The center of the vortex is slightly shifted towards the upper part of the Te-enriched solution (i.e., towards the dissolution interface).

The obtained data show that an increase in the thickness of the tellurium layer promotes the transition from laminar to vortex flows at $Ra_T/Ra_C \approx 1 \cdot 10^{-2}$. The results in Tables 2, 3, and Fig. 3 allow us to estimate the ranges of parameters that ensure conditions close to optimal. This approach allows for faster selection of specific technological parameters and reduces the number of required growth experiments.

The resulting temperature distribution and the structure of the convective flow simultaneously depend on thermogravitational and concentration convection. The latter, in turn, is caused by density disturbances in the Te-enriched solution. The driving force of thermogravitational convection is the temperature gradient (numerator in equation (28)). Thermogravitational convection is opposed by viscosity and thermal diffusivity, as shown in the denominator of (28). For concentration convection, the driving force (concentration gradient) is opposed by viscosity and molecular diffusion. Accordingly, the characteristics of these phenomena are expressed through the thermal Rayleigh number (28) and the concentration Rayleigh number (31).

$$Ra_T = \frac{g\beta_T \Delta T L^3}{\nu\alpha}, \quad (28)$$

$$\nu = \frac{\mu}{\rho}, \quad (29)$$

$$\alpha = \frac{k}{\rho c_P}, \quad (30)$$

$$Ra_C = \frac{g\beta_C \Delta C L^3}{\nu D}, \quad (31)$$

where, Ra_T is the Rayleigh temperature number; Ra_l is the Rayleigh concentration number; $g = 9.8 ms^{-2}$ is the acceleration due to gravity; β_T is the temperature coefficient of volumetric expansion; β_C is the coefficient that accounts for changes in density with concentration; $\Delta T, \Delta C$ are the temperature and concentration gradients, respectively; L is the characteristic size of the Te-enriched solution zone; ρ is the density; c_P is the specific heat capacity at constant pressure; ν, μ are the kinematic and dynamic viscosity coefficients, respectively; α is the thermal diffusivity; k is the thermal conductivity coefficient.

The ratio of (28) to (31) shows the relative contributions of thermogravitational and concentration convection to the heat and mass transfer process in the Te-enriched solution layer.

$$\frac{Ra_T}{Ra_C} = \frac{\beta_T \Delta T D}{\beta_C \Delta C \alpha} \quad (32)$$

When $Ra_T / Ra_l > 1$, thermogravitational convection dominates, and the movement of the solution is mainly determined by temperature gradients. When $Ra_T / Ra_l < 1$, the flow structure and intensity are determined by the concentration gradients of CZT dissolved in tellurium.

Analysis of (32) shows that changing the Ra_T / Ra_l ratio is possible only by adjusting the parameters ΔT and ΔC, since only they are available for change by selecting geometric and technological parameters, temperature distribution, etc. The remaining parameters are material properties and are generally immutable. From this, several directions for optimizing the technological parameters of CZT crystal growth by the THM method can be identified. Additionally, where possible, we provide estimates of the Ra_T / Ra_l ratio based on data from the cited works (the authors of those works do not provide or analyze the Ra_T / Ra_l ratio).

1. Changing the temperature gradient by simultaneously increasing the amplitude and width of the temperature peak. This approach does not lead to a change in the Ra_T / Ra_l ratio. At the same time, two processes occur. On the one hand, changing the temperature peak causes a change in the numerator of (32) due to the temperature difference ΔT. On the other hand, a change in the concentration difference ΔC also occurs. Additionally, we take into account that the concentration and temperature are interrelated (determined along the liquidus line of the binary phase diagram (22)) and that equilibrium CZT concentration is established at the dissolution and crystallization fronts (21). As a result, ΔT and ΔC change almost proportionally, and the Ra_T / Ra_l ratio remains unchanged.

2. Changing the Ra_T / Ra_l ratio by independently adjusting the amplitude and width of the temperature peak. This approach allows the Ra_T / Ra_l ratio to be changed. Let us illustrate this with an example. Changing the amplitude of the temperature peak primarily results in a change in the temperature difference ΔT. The change in the concentration difference ΔC will be determined by the width of the temperature peak, specifically by the temperature values at the dissolution and crystallization interfaces (for reasons mentioned in the previous point). Thus, it becomes possible to purposefully control the Ra_T / Ra_l ratio. This option is considered in [22] (estimated $Ra_T / Ra_l = 4 \cdot 10^3$). It is also envisaged that control of the Ra_T / Ra_l ratio can be achieved by asymmetrically positioning the temperature peak relative to the Te-enriched solution zone [24]. This approach is well implemented in EDG furnaces.

3. Changing the ratio Ra_T / Ra_l through accelerated crucible rotation. In [40], among other things, it is noted that the Accelerated Crucible Rotation Technique (ACRT) significantly improves the quality of CZT ingots grown using the Cold Traveling Heater Method. To explain this, the authors refer to the concept of the Ekman layer [51]. They also point out that natural convection is the dominant mechanism of mass transfer in the CTHM method, but it is difficult to control. To create a controlled regime of forced convection, ACRT is applied [52, 40]. According to [20], the estimated $Ra_T / Ra_l = 3.9 \cdot 10^{-3}$, and in [40] the estimated $Ra_T / Ra_l = 2.7 \cdot 10^{-3}$.

4. Reducing Ra_T by applying an external magnetic field. The magnetic field reduces the Ra_T / Ra_l ratio. The resulting Lorentz force counteracts the liquid motion caused by temperature gradients. At the same time, molecular diffusion transfer is suppressed to a much lesser extent. This is due to the fact that molecular diffusion processes occur significantly slower than thermal processes. This approach is developed in [19], with an estimated $Ra_T / Ra_l = 7 \cdot 10^{-3}$ [23].

5. Changing the flow structure. It is based on the fact that the flow structure significantly depends on the temperature gradient and the width of the Te-enriched solution zone (28). At Ra_T values below the critical value, convective flows are laminar. As Ra_T approaches the critical value, the flow structure becomes more complex [53]. In particular, additional vortices appear (Fig. 3h). Such a complication of the flow structure hinders mass transport because the material exchange between two vortices through convection is weakened [54].

It should be separately noted that in [24,25, 52], the estimated $Ra_T / Ra_l > 1$. This likely indicates significantly different growth conditions.

Summarizing the data presented above and noting their good agreement with the results

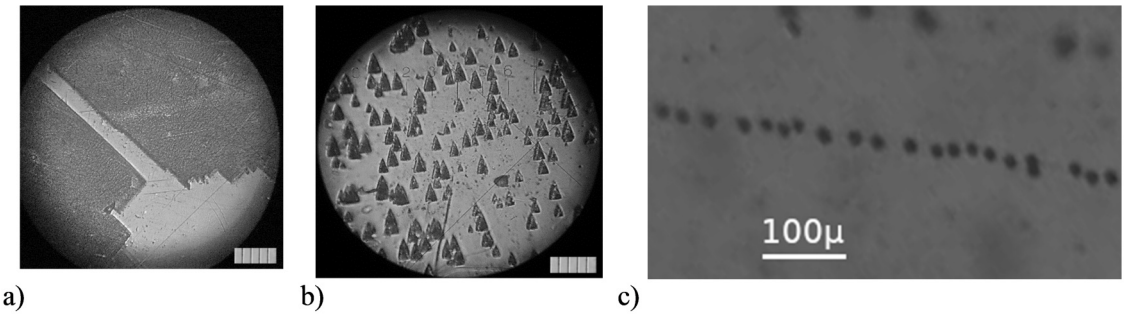

Fig. 4. Temperature distribution and flow structure in the melt with the Te-enriched solution thickness of 40 mm. Microstructure of $Cd_{0.9}Zn_{0.1}Te$ crystal cross-sections revealed by chemical polishing (a) and selective etching (b). IR image of Te inclusions decorating the grain boundary (c).

of our modeling, the following conclusions can be drawn. The proposed criterion of the Ra_T / Ra_l ratio in the range from $1 \cdot 10^{?3}$ to $1 \cdot 10^{?2}$ can serve as a simple tool for characterizing growth conditions close to optimal. This criterion is also valuable for solving optimization problems aimed at determining the thermal conditions necessary for growing high-quality CdTe and CZT crystals. Its application is possible in various variants of the THM method, including ampoule rotation and the use of a magnetic field. Furthermore, the proposed criterion connects the main technological parameters by means of the simple ratio: temperatures and concentrations near the dissolution and crystallization interfaces, and the thickness of the tellurium layer. It can be used for quick approximate calculations, making it a universal tool for analysis and modeling tasks. Controlling the Ra_T / Ra_l ratio and maintaining it within the specified range allows optimizing growth conditions, for example, by separately managing thermogravitational and concentration convection.

3.3. Crystal Growth

To validate the calculations, a series of experimental ingots of $Cd_{0.9}Zn_{0.1}Te$ solid solutions was grown. The starting material was synthesized by melting the initial elements (Cd, Zn, Te) taken in stoichiometric proportions. The synthesized material was loaded into a quartz ampoule with a carbon coating, along with elemental tellurium. The loaded ampoule was evacuated and sealed. The ingots were grown at a rate of 0.1 – 0.2 mm/hr.

At low Ra_T / Ra_l values of approximately $1 \cdot 10^{-?}$, numerous tellurium inclusions are observed in the grown ingot. The size of some inclusions reaches hundreds of microns. Near such large inclusions, grain boundaries with significant misorientation are detected. The composition of these inclusions, measured by

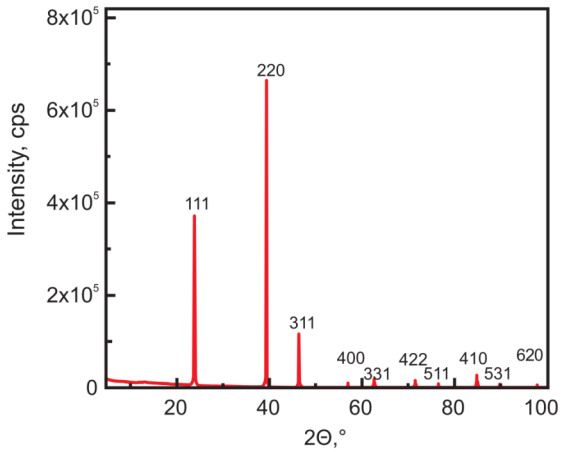

Fig. 5. Powder XRD pattern for $Cd_{0.9}Zn_{0.1}Te$.

electron microscopy with X-ray microanalysis, showed a tellurium concentration of 90–100 at.%. This is a result of morphological instability at the crystallization interface. The number of blanks suitable for manufacturing spectroscopic grade detectors is very small.

At the Ra_T / Ra_l values greater than $3 \cdot 10^{-2}$, fewer tellurium inclusions are observed in the grown ingots compared to $Ra_T / Ra_l \approx 1 \cdot 10^{-?}$. The typical sizes of inclusions range from 5 to 20 microns. The subgrain boundary network is quite pronounced. Macrodefects are absent. As in the previous case, the number of blanks suitable for manufacturing spectroscopic grade detectors is also small.

The best results (among the series of grown ingots) were achieved at Ra_T / Ra_l values from $1 \cdot 10^{-3}$ to $1 \cdot 10^{-2}$. In this case, the crystallization interface is slightly convex towards the melt. The resulting ingots exhibit a relatively small number of tellurium inclusions, which are arranged in planes and decorate the crystallization interface at the time of their formation.

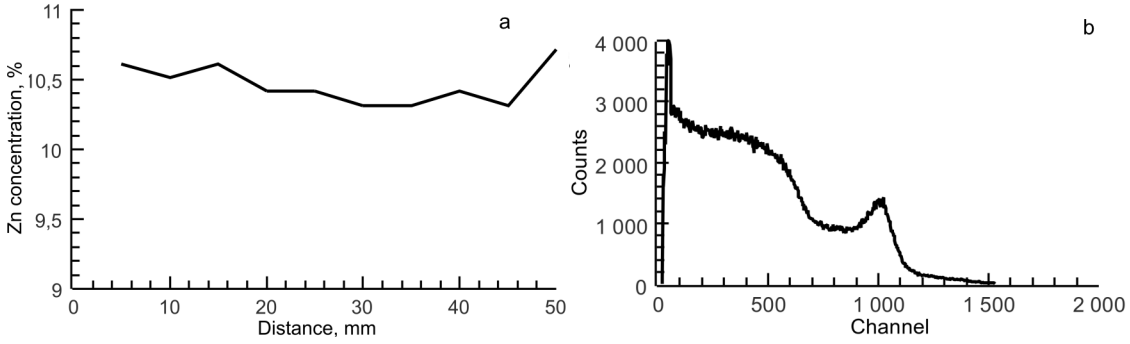

Fig. 6. Zn distribution along the ingot axis (a) and the amplitude spectrum (b)

Such ingots are suitable for manufacturing spectroscopic grade detectors.

The characterization of the distribution and size of grains present in all investigated samples of the crystals was performed using the chemical etching method. A chemical polishing solution was used for this purpose. For example, Fig. 5(a) shows a typical microstructure of a $Cd_{0.9}Zn_{0.1}Te$ sample.

Selective chemical etching revealed dark triangular-shaped etch pits perpendicular to the growth direction, over the entire surface of the cut (Fig. 5(b)). The revealed etch pits are growth dislocations decorated by impurities. In areas of their highest concentration, the dislocation density, estimated by counting the etch pits, varied within a certain range. The results of the IR microscopy study of the grown ingots showed the absence of other phase inclusions and gas inclusions in the ingot. Inclusions observed in the ingot volume are shown in Fig. 5(c).

The phase composition of the obtained $Cd_{0.9}Zn_{0.1}Te$ in the nose part of the ingot was studied using X-ray diffraction (XRD). For this, the grown ingots were carefully crushed and homogenized. Figure 5 shows the powder XRD pattern of the nose part of the ingot. The sharp diffraction peaks confirm the crystallinity of the grown ingot. The XRD pattern indicates the presence of single-phase CZT with a cubic lattice and the absence of a hexagonal phase.

The distribution of Zn along the ingot axis is shown in Fig. 6(a). A fairly uniform distribution is observed, which is typical for ingots obtained by the THM method. To evaluate the spectroscopic characteristics, a detector with dimensions of 5×5×5 mm^3 was fabricated from the ingot. Au electrodes were deposited on the surface of the detector by chemical deposition. The measured energy resolution at the 662 keV line of the ^{13}Cs source was 7.3%. The corresponding amplitude spectrum is shown in Fig. 6(b).

4. Conclusion

A numerical model proposed in this work allows determining parameters close to optimal for the growth of $Cd_{0.9}Zn_{0.1}Te$ crystals by the THM method in a multi-zone EDG furnace.

It was established that, to achieve growth conditions close to optimal, the ratio of the thermal Rayleigh number (Ra_T) to the concentration Rayleigh number (Ra_C) should be maintained in the range from $1 \cdot 10^{-3}$ to $1 \cdot 10^{-2}$.

It was shown that the best results are achieved with a slightly convex crystallization interface. The quality of the ingots grown under the calculated conditions allows the production of spectroscopic grade detectors.

The proposed Ra_T / Ra_l ratio criterion can be applied to optimize thermal conditions in various modifications of the THM method, including ampoule rotation and the application of a magnetic field.

The proposed numerical modeling and optimization of growth conditions makes it possible to significantly reduce the number of experimental growths needed to obtain high-quality spectroscopic detectors.

References

1. U. Cevik, E. Bacaksiz, N. Damla et al., Radiat. Meas. **43**, 8, 1437, (2008). https://doi.org/10.1016/j.radmeas.2008.03.033
2. S. Del Sordo, L. Abbene, E. Caroli et al., Sensors **9**, 3491 (2009). https://doi.org/10.3390/s90503491
3. A. E. Bolotnikov, S. Babalola, G. S. Camarda *et al*., in *IEEE Trans Nucl Sci*, **58**, (4), 1972 (2011). https://doi.org/10.1109/TNS.2011.2160283.
4. U. N. Roy, G. Camarda, Y. Cui et al., Appl. Phys. Lett. **114**, 232107 (2019). https://doi.org/10.1063/1.5109119

5. J.S. Yadav, S. Savitri, J.P. Malkar NIM A **552,** (2005). https://doi.org/10.1016/j.nima.2005.07.001
6, S. U. Egarievwe U. Roy; E. Agbalagba et al., IEEE Access, **8**, 137530 (2020). https://doi.org/10.1109/ACCESS.2020.3012040
7. Schillebeeckx, P., Borella, A., Bruggeman, et al., Cadmium Zinc Telluride Detectors for Safeguards Applications. In: K. Iniewski, (eds) Advanced Materials for Radiation Detection. Springer, Cham. (2022). https://doi.org/10.1007/978-3-030-76461-6_15
8. K. Iniewski *JINST,* **9**, C11001 (2014). https://doi.org/10.1088/1748-0221/9/11/C11001.
9. C. G. Wahl, W. Kaye, F. Zhang et al., 2017 IEEE NSS/MIC, Atlanta, GA, USA, 2017, p.1. https://doi.org/10.1109/NSSMIC.2017.8532778
10. F. Doty, J. Butler, J. Schetzina et al., J Vac. Sci. Technol., **B10**, 1418, (1992) https://doi.org/10.1116/1.586264
11. T. Takahashi, S. Watanabe, IEEE Trans Nucl Sci **48**(4), 950, (2001). https://doi.org/10.1109/23.958705
12. V. Komar, A. Gektin, D. Nalivaiko et al., NIM A **458** (1-2), 113, (2001). https://doi.org/10.1016/S0168-9002(00)00856-1
13. B. Hong, S. Zhang, L. Zheng et al., J. Cryst. Growth **546**, 125776, (2020). https://doi.org/10.1016/j.jcrysgro.2020.125776
14. W. Wu, J. Zhang, L. Wang et al., Phys. Status Solidi C, **13**, 408 (2016). https://doi.org/10.1002/pssc.201510226
15. U.N. Roy, A. Burger, R.B. James, J. Cryst. Growth, **379**, 57, (2013). https://doi.org/10.1016/j.jcrysgro.2012.11.047
16. K. Schwenkenbecher, P. Rudolph, Cryst. Res. Technol. **20**, 1609 (1985). https://doi.org/10.1002/CRAT.2170201212
17. L. Yin, W. Jie, T. Wang, J. Cryst. Growth, **461**, 16, (2017) https://doi.org/10.1016/j.jcrysgro.2016.11.074
18. U.N. Roy, S. Weiler, J. Stein, J. Cryst. Growth, **312**, 2840, (2010) https://doi.org/10.1016/j.jcrysgro.2010.05.046
19. Y. Liu, S. Dost, B. Lent et al., J. Cryst. Growth, **254**, 285, (2003) https://doi.org/10.1016/S0022-0248(03)01140-0
20. S. Dost, Y. Liu, *Comptes Rendus Mécanique*, **335** (5–6), (2007), doi: 10.1016/j.crme.2007.05.011
21. C. W. Lan и D. T. Yang, *Modelling Simul. Mater. Sci. Eng.*, **3**, (1), (1995), doi: 10.1088/0965-0393/3/1/007
22. S. Dost, R. A. Meric, B. Lent *Trans. Can. Soc. Mech. Eng.*, **24**, (1B), (2000), doi: 10.1139/tcsme-2000-0006
23. B. Lent, S. Dost, R. F. Reddenet et al., *J. Cryst. Growth,* **237–239**, (2002), doi: 10.1016/S0022-0248(01)02208-4
24. X. Ye, B. Tabarrok, D. Walsh, *J. Cryst. Growth*, **169**, (4), (1996), doi: 10.1016/S0022-0248(96)00451-4
25. J. H. Peterson, M. Fiederle, J. J. Derby, *J. Cryst. Growth*, **454**, (2016), doi: 10.1016/j.jcrysgro.2016.08.055
26. M. D. Reed, Cs. Szeles, S. E. Cameron, *J. Cryst. Growth*, **289**, (2), (2006), doi: 10.1016/j.jcrysgro.2005.12.103
27. C. Szeles, S. E. Cameron, J.-O. Ndap, et al., «Advances in the crystal growth of semiinsulating CdZnTe for radiation detector applications», в *2001 IEEE Nuclear Science Symposium Conference Record (Cat. No.01CH37310)*, San Diego, CA, USA: IEEE, 2002, cc. 2424–2428. doi: 10.1109/NSSMIC.2001.1009309.
28. J. J. Derby D. Gasperino, «Computational Models for Crystal Growth of Radiation Detector Materials: Growth of CZT by the EDG Method», *MRS Proc.*, т. 1038, cc. 1038-O05-09, 2007, doi: 10.1557/PROC-1038-O05-09
29. L. Lun, A. Yeckel, M. Reed, C. Szeles, et al., *J. Cryst. Growth*, **290**, (1), (2006), doi: 10.1016/j.jcrysgro.2006.01.006
30. D. Gasperino, M. Bliss, K. Jones, *J. Cryst. Growth*, **311**, (2009), doi: 10.1016/j.jcrysgro.2009.01.141.
31. C. Szeles, S. E. Cameron, S. A. Soldner, et al., *J. Electron. Mater.*, **33**, (6), (2004), doi: 10.1007/s11664-004-0076-z
32. D. Brellier *J. Electron. Mater.*, **43**, (8), (2014), doi: 10.1007/s11664-014-3146-x.
33. Y. Okano, S. Nishino, S. Ohkubo, *J. Cryst. Growth*, **237–239**, (2002), doi: 10.1016/S0022-0248(01)02339-9
34. Yu. D. Filatov, V. I. Sidorko, S. V. Kovalev, *J. Superhard Mater.*, **43**, (4), (2021), doi: 10.3103/S1063457621040043
35. M. Inoue, I. Teramoto, и S. Takayanagi, *J. Appl. Phys.* **33**, (8), (1962), doi: 10.1063/1.1729023
36. E. Garnier, N. Adams, и P. Sagaut, «LES Governing Equations», (2009), doi: 10.1007/978-90-481-2819-8_2
37. G. Katul, L. Mahrt, D. Poggi, et al., *Boundary-Layer Meteorology*, **113**, (2004), doi: 10.1023/B:BOUN.0000037333.48760.e5
38. S. Verdério Júnior, V. Scalon, et al., *Ingeniare. Revista chilena de ingeniería*, **26**, (2018(, doi: 10.4067/S0718-33052018000400546
39. Y. P. Almeida, P. L. C. Lage, L. F. L. R. Silva, *Appl. Therm. Eng.,***81**, (2015), doi: 10.1016/j.applthermaleng.2015.02.027.

40. A. El Mokri, R. Triboulet, A. Lusson, et al., *J. Cryst. Growth*, **138**, (1), (1994), doi: 10.1016/0022-0248(94)90800-1.
41. C.-H. Su, *AIP Advances*,**5,** (5), (2015), doi: 10.1063/1.4921025
42. C. Martinez-Tomas, V. Muñoz, и R. Triboulet, *J. Cryst. Growth*, **197**, (3), (1999), doi: 10.1016/S0022-0248(98)00806-9.
43. M. Divecha *J. Cryst. Growth*, (468) (2017). https://doi.org/10.1016/j.jcrysgro.2016.09.068
44. J. Peterson, «Understanding growth rate limitations in production of single-crystal cadmium zinc telluride (CZT) by the traveling heater method (THM)», 2017. Thesis (Ph.D.)--University of Minnesota, 2017.; Publication Number: AAT 10261040; ISBN: 9780355061239; Source: Dissertation Abstracts International, Volume: 78-11(E), Section: B.; 133 p.
45. C. K. Ghaddar, C. K. Lee, S. Motakef, et al., *J. Cryst. Growth*, **205**, (1), (1999), doi: 10.1016/S0022-0248(99)00206-7
46. V. Kumar, S. Dost, F. Durst, *Appl. Math. Model.* **31**, (3,) (2007), doi: 10.1016/j.apm.2005.11.022
47. S. C. Mishra, H. K. Roy, J. Comput. Phys. **223**, (1), c(2007), doi: 10.1016/j.jcp.2006.08.021
48. M. Tano-Retamales, P. Rubiolo, O. Doche, «Development of Data-Driven Turbulence Models in OpenFOAM: Application to Liquid Fuel Nuclear Reactors», в *OpenFOAM®: Selected Papers of the 11th Workshop*, J. M. Nóbrega и H. Jasak, Ред., Cham: Springer International Publishing, 2019, cc. 93–108. doi: 10.1007/978-3-319-60846-4_7.
49. V. da Silva, G. de Neves Gomes, A. de Lima e Silva et al., *Heat Mass Transf.* **55**, 2289 (2019). https://doi.org/10.1007/s00231-019-02574-5
50. M. Abbassi, D. Lahaye, K. Vuik, Modelling Turbulent Combustion Coupled with Conjugate Heat Transfer in OpenFOAM. In: F. Vermolen, C. Vuik, (eds) Numerical Mathematics and Advanced Applications ENUMATH 2019. Lecture Notes in Computational Science and Engineering, 139. Springer, Cham (2019). https://doi.org/10.1007/978-3-030-55874-1_113
51. E. O. Schulz-Dubois, *J. Cryst. Growth* **12**, (2), (1972), doi: 10.1016/0022-0248(72)90034-6.
52. L. Yin, W. Jie, T. Wang, B. Zhou,et al., *J. Wuhan Univ. Technol.-Mat. Sci. Edit.*, **32**, (2), (2017), doi: 10.1007/s11595-017-1602-1.
53. W. L. Heitz и J. W. Westwater, *J Heat Trans*, **93**, (2), (1971), doi: 10.1115/1.3449783.
54. X. Wang, W. Yuchi, J. Zhu,et al., *J. Therm. Sci.*, **30**, (5), (2021), doi: 10.1007/s11630-021-1418-3.